ADVANCED MATERIALS
www.advmat.de

Highly-Adaptable Optothermal Nanotweezers for Trapping, Sorting, and Assembling across Diverse Nanoparticles

Jiajie Chen, Jianxing Zhou, Yuhang Peng, Xiaoqi Dai, Yan Tan, Yili Zhong, Tianzhong Li, Yanhua Zou, Rui Hu, Ximin Cui, Ho-Pui Ho, Bruce Zhi Gao, Han Zhang, Yu Chen, Meiting Wang, Xueji Zhang, Junle Qu,* and Yonghong Shao**

Optical manipulation of various kinds of nanoparticles is vital in biomedical engineering. However, classical optical approaches demand higher laser power and are constrained by diffraction limits, necessitating tailored trapping schemes for specific nanoparticles. They lack a universal and biocompatible tool to manipulate nanoparticles of diverse sizes, charges, and materials. Through precise modulation of diffusiophoresis and thermo-osmotic flows in the boundary layer of an optothermal-responsive gold film, highly adaptable optothermal nanotweezers (HAONTs) capable of manipulating a single nanoparticle as small as sub-10 nm are designed. Additionally, a novel optothermal doughnut-shaped vortex (DSV) trapping strategy is introduced, enabling a new mode of physical interaction between cells and nanoparticles. Furthermore, this versatile approach allows for the manipulation of nanoparticles in organic, inorganic, and biological forms. It also offers versatile function modes such as trapping, sorting, and assembling of nanoparticles. It is believed that this approach holds the potential to be a valuable tool in fields such as synthetic biology, optofluidics, nanophotonics, and colloidal science.

1. Introduction

Optical tweezers have made outstanding contributions to the research of single particle analysis and deepened human understanding of the nano-world since its invention by Arthur Ashkin, and it was awarded the Nobel Prize in Physics in 2018.[1,2] Particularly, the precise and non-contact manipulation capabilities of optical tweezers have significantly contributed to the advancements in biophotonic applications.[3,4] Traditional optical tweezers depend on optical momentum transfer to produce gradient forces,[5] enabling 3D manipulation. Pioneering efforts have significantly extended the scope of trapping diverse nanoparticles, including biological and metallic particles, into the nanoscale realm.[6–11] However, traditional optical tweezers require high laser power density and the spatial resolution is limited by diffraction. In the past decade, different approaches that cooperate with other fields such as plasmonics,[12] metamaterials,[13] electrophoresis,[14–18] optofluidics,[19–25] or thermophoresis[26,27] have redeemed the disadvantages of traditional optical tweezers and expanded the range of physical properties of the trappable nanoparticles.

For example, researchers have developed various types of plasmonic tweezers that can trap bio-nanoparticles near a nanostructure beyond the diffraction limit.[12,28] However, achieving large-scale nanoparticle transportation and manipulation through plasmonic tweezers remains challenging. Nevertheless, optothermal tweezers, in which optical-induced thermodynamic forces are adopted, have been developed to manipulate nanoparticles on a large scale at subwavelength precision.[29–40] The power density required for optothermal tweezers is three

J. Chen, J. Zhou, Y. Peng, X. Dai, Y. Zhong, T. Li, Y. Zou, R. Hu, H. Zhang, Y. Chen, M. Wang, J. Qu, Y. Shao
State Key Laboratory of Radio Frequency Heterogeneous Integration
Key Laboratory of Optoelectronic Devices and Systems of Ministry of Education and Guangdong Province
College of Physics and Optoelectronics Engineering
Shenzhen University
Shenzhen 518060, China
E-mail: cjj@szu.edu.cn; jlqu@szu.edu.cn; shaoyh@szu.edu.cn

Y. Tan, X. Zhang
School of Biomedical Engineering
Shenzhen University
Shenzhen 518060, China

X. Cui
State Key Laboratory of Radio Frequency Heterogeneous Integration
College of Electronics and Information Engineering
Shenzhen University
Shenzhen 518060, China

H.-P. Ho
Department of Biomedical Engineering
The Chinese University of Hong Kong
Shatin 999077, Hong Kong

B. Z. Gao
Department of Bioengineering and COMSET
Clemson University
Clemson, SC 29634, USA

The ORCID identification number(s) for the author(s) of this article can be found under https://doi.org/10.1002/adma.202309143

DOI: 10.1002/adma.202309143

orders of magnitude lower than that of the traditional optical tweezers.[31,33,34,38,39] However, these methods were limited to specific nanoparticles with negative surface charges.[41] Recently, alternative methods were introduced involving the use of ionic surfactants to induce thermophoresis in particles, allowing their trapping at the laser heating center.[32,37,42] While the use of ionic surfactants can alter and modify the surface charge of the target particles, limiting its broader applications in manipulating bio-nanoparticles. The diffusiophoresis[43,44] induced by nonionic surfactant (PEG) has also proven instrumental in facilitating aggregations of DNA and proteins,[45–49] manipulation of micro-sized particles (0.3–10 μm) or cells.[50–52] However, the precise manipulation of nanoparticles (5–200 nm) across different materials for micrometer scale transportation range has remained unattainable. A universal optothermal trapping, sorting, and assembling approach that accommodates diverse particles in varying materials, surface charges, sizes, and shapes is lacking. Currently, one typically needs to design specific trapping strategies tailored for different types of particles, such as biological or metal nanoparticles.[22,34,53–56]

In addressing these challenges, by incorporating diffusiophoresis with the thermo-osmotic flow, that is, a slip flow parallel to the solid–liquid interface induced by the excess enthalpy in the boundary layer,[57] we developed highly-adaptable optothermal nanotweezers (HAONT), enabling nanoparticle manipulation with sub-10 nm trapping accuracy without surface modification. This technique operates effectively on a wide range of nanoparticles, encompassing organic, inorganic, and biological entities, such as polystyrene spheres (PSs), mesoporous silica nanoparticles (MSNs), quantum dots (QD), metal nanoparticles (ranging from 5 to 200 nm), exosomes, viruses (including COVID-19), and bacteria (*Escherichia coli* cell). HAONT scheme also offers versatile capabilities for nanoparticle trapping, sorting, and assembling. Furthermore, we also systematically studied the size dependency of the metal nanoparticle-induced ∇T homogenization effect, serving as a valuable reference for other researchers engaged in optothermal tweezers. Additionally, by simply increasing the laser power, we've established a novel optothermal doughnut-shaped vortex (DSV) trapping strategy, facilitating a new physical interaction mode between cells and nanoparticles. Therefore, this nanotweezers system represents a highly versatile solution, boasting exceptional biocompatibility, precise trapping capabilities, and an extensive transportation range. These attributes make it well-suited for a wide range of applications in the field of nanotechnology and biophotonics.

2. Results and Discussion

2.1. Working Principle

As shown in **Figure 1a**, HAONT operates within a microfluidic chamber containing a thin layer of gold (Au) film on the glass bottom. To facilitate HAONT, a water-soluble, nonionic, biocompatible polymer of polyethylene glycol (PEG, molecular weight M_w = 10 000) is introduced into the aqueous solution. PEG is a widely used biological surfactant known for its good biocompatibility.[58,59] It retains its thermal stability below 100 °C.[60] Following laser heating of the Au film, as depicted in Figure 1b,c, temperature fields are generated (measurement method detailed in Note S1, Supporting Information). This temperature gradient gives rise to two major thermodynamic forces: Diffusiophoretic force (F_D) and thermo-osmotic force (F_{TO}). When the resulting net forces (F_{Net}) acting on the nanoparticles are directed toward the center of the laser spot on the Au film, trapping is initiated. Diffusiophoresis is an interfacial force that can induce motions in colloidal nanoparticles due to osmotic stress in the vicinity of the nanoparticle surface.[43,44] In our scheme, under the optically induced thermal gradient (∇T), the PEG molecules undergo thermophoresis, migrating from a hot to a cold region, and the thermophoresis of the PEG molecule causes the diffusiophoresis of the nanoparticle towards the hot region due to particle-polymer boundary interaction. Therefore, the total transport velocity of the particle is (see Note S2, Supporting Information).[43,61]

$$v = -\left[D_T - \frac{k_B}{3\eta} R_g^2 c N_A \left(TS_T^m - 1\right)\right] \nabla T = -\left[D_T + D_T^{PEG}\right] \nabla T \quad (1)$$

where D_T is thermophoretic mobility of the particle in water, k_B is Boltzmann constant, N_A is Avogadro constant, and η is solution viscosity. The parameters concerning the PEG molecule, denoted as c, S_T^m, and R_g, represent the concentration in mol L^{-1}, the Soret coefficient, and the gyration radius, respectively. For example, in the case of PEG-10000 (molecular weight M_w = 10 000 g mol^{-1}), at a mass fraction of 5%, viscosity η is 2.57 × 10^{-3} Pa s,[62] $R_g = 0.02 M_w^{0.58}$ (≈4.2 nm),[63] and S_T^m is 0.064 1/K.[64] We can find −1.7 μm^2 K^{-1} s^{-1} for the diffusiophoresis term D_T^{PEG} whose absolute value is larger than the of nanoparticle's thermophoretic mobility ($D_T \approx 0.1$ μm^2 K^{-1} s^{-1}).[35] Therefore, the PEG-assisted overall thermophoretic mobility ($D_T + D_T^{PEG}$) is negative, that is, the nanoparticle can be driven to the heating center via the dominant force from diffusiophoresis. Note that the above discussion is conducted without considering the influence of thermoelectrical field generation from water molecules,[41,65] which is a negligible factor in the HAONT scheme. Nevertheless, contributions from thermophoresis of charged particles and water molecules are discussed in Note S3, Supporting Information.

In the vicinity of the solid-liquid interface, a micrometer-scale toroidal slip flow (indicated by the gray arrows in Figure 1b,c), known as thermo-osmotic flow, also contributes to the trapping of nanoparticles.[35] It originates from the excess enthalpy h in the solid-liquid interface due to the temperature gradient. The thermo-osmotic flow velocity v_{TO} is described as follows.[57]

$$v_{TO} \cdot \hat{t} = \chi \frac{\nabla T}{T} \cdot \hat{t} \quad (2)$$

where $\hat{t}$ is a unit vector tangential to the Au-liquid interface and χ is the thermo-osmotic coefficient. When χ is positive, liquid flows towards the hot side at the interface. In our case, the thermo-osmotic coefficients of AuNS and PS are χ_{Au} = 3.9 × 10^{-10} $m^2 \cdot s^{-1}$ and χ_{PS} = 1.6 × 10^{-10} $m^2 \cdot s^{-1}$ respectively (see Note S4, Supporting Information for details). Note that natural convective flow is suppressed due to the shallower chamber height (30 μm).[66,67]

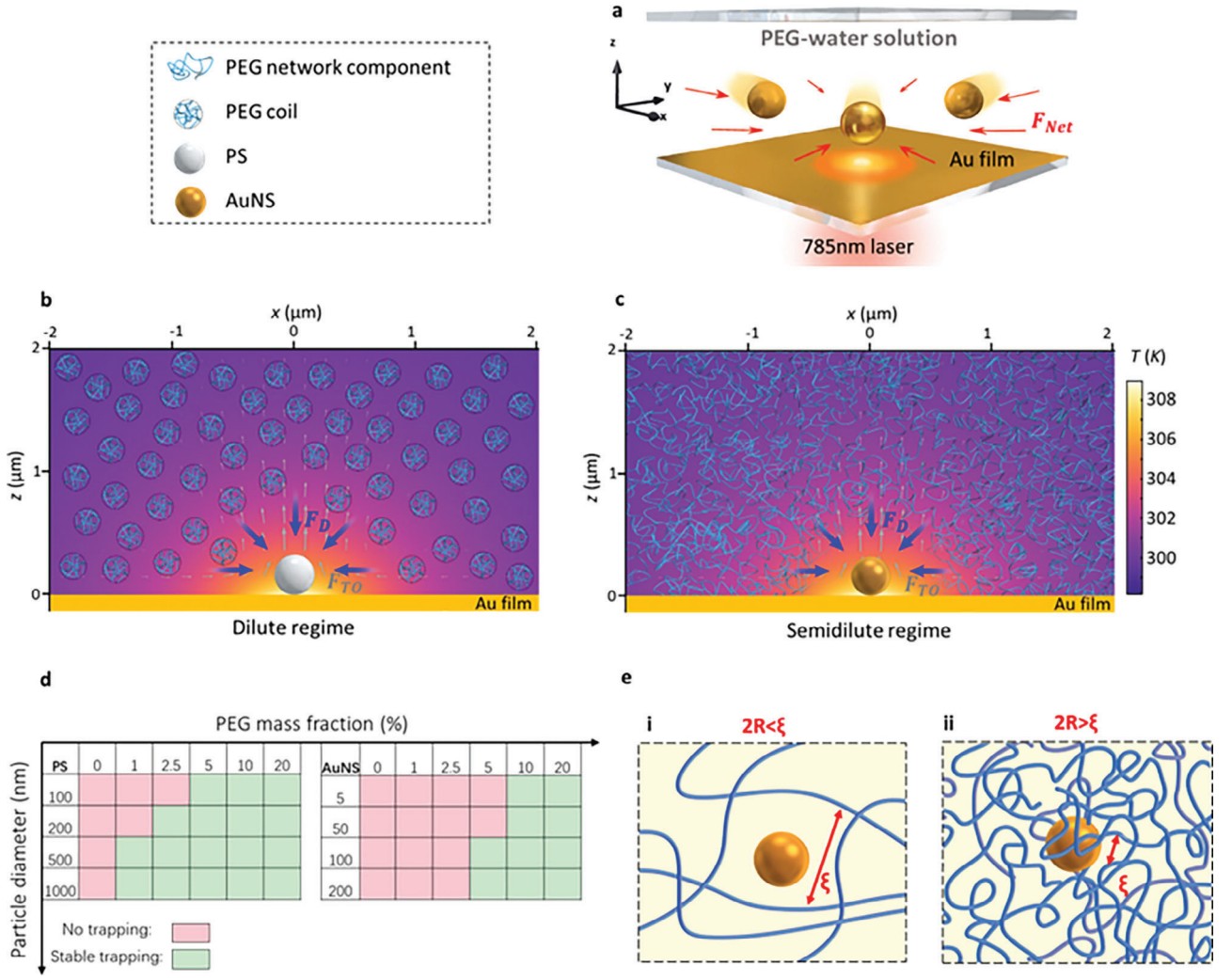

Figure 1. The working principle of HAONT. a) The microfluidic channel consists of two cover glass slides, and the bottom one is coated with 10 nm Au film and a 5 nm chromium adhesion layer. The height of the chamber is 30 μm. The F_{Net} is the net force for nanoparticle manipulation. b) Polystyrene sphere (PS) trapping in dilute PEG solution. c) Gold nanosphere (AuNS) trapping in semidilute PEG solution. The gray and blue arrows indicate the thermo-osmotic force (F_{TO}) and diffusiophoretic force (F_D) respectively. The incident 785 nm laser spot diameter is 1 μm, and the incident optical power is 0.3 mW. d) Trapping diagram for PS and AuNS particles of varying sizes in different PEG concentrations, all exhibiting neutral surface charges. e) Material modalities when an AuNS (radius = R) is present in a PEG network with different correlation lengths ξ.

2.2. Nanoparticle Trapping and Assembling

Trapping behaviors are affected by PEG concentration, as PEG molecules disperse in the solvent in a concentration-dependent manner, falling into three distinct regimes. If the PEG volume fraction ϕ is below its critical volume fraction ϕ^* ($\phi < \phi^*$), that is, dilute regime (see Figure 1b), the polymer molecules can be regarded as coiled spheres with gyration radius of R_g. If ϕ is larger than its critical volume fraction ϕ^* ($\phi^* < \phi < \phi_e$, ϕ_e is the entanglement volume fraction), as depicted in Figure 1c, the PEG polymer is in a semidilute regime,[68] where the PEG molecule coils start to merge and the polymer chains are gradually entangled with each other. And we can calculate that ϕ^*= 4.7% and ϕ_e = 29.9% for PEG (10K), and our experiments are within the regime of dilute and semidilute (see Note S5, Supporting Information for details). As the trapping status diagram in Figure 1d shows, in our experiments, at a dilute regime (≤ 5%), a fraction of PS can be trapped and AuNS can be hardly trapped. We attribute this to the temperature field homogenization induced by the larger thermal conductivity of metal nanoparticles (see Note S6, Supporting Information for details).[69] In the case of a semidilute solution regime (Figure 1c), where the polymer concentration is above the critical volume fraction (ϕ^*), both PS and AuNS can be easily trapped. In this regime, the PEG molecules form a 2D network of overlapping polymer chains (or polymer blobs). It can be characterized by an average mesh size called the correlation length ξ, which is a decreasing function of polymer volume fraction ϕ ($\xi \approx R_g(\phi^*/\phi)^{0.75}$).[70] Therefore. For PEG mass fractions at 5%, 10%, and 20%, the calculated correlation lengths ξ are about 4.2, 2.6, and 1.4 nm respectively. Here, we can treat the PEG molecules as smaller polymer network fragments in the length scale of ξ, and diffusiophoresis can act

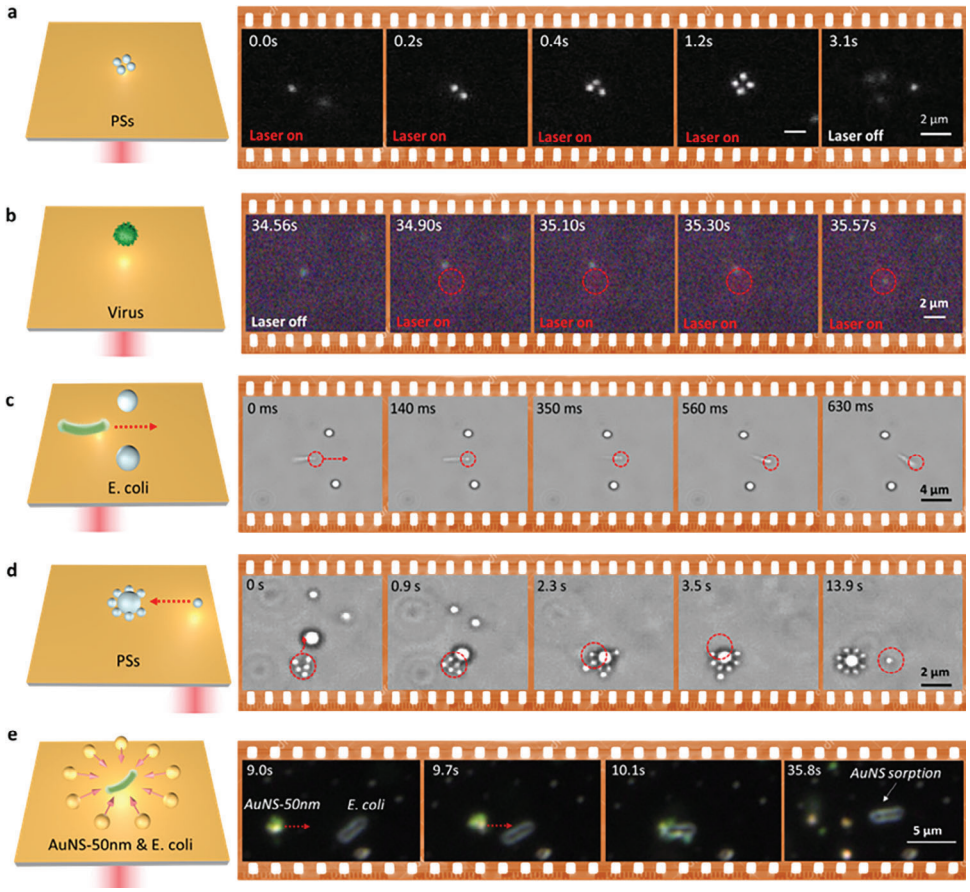

Figure 2. Schematic figures and successive microscope frames showing nanoparticles trapping and assembling. a) Dynamic trapping and releasing of 200 nm PS, the laser is turned off at 3.1s, and the video is recorded by dark-field microscopy. b) Single 2019-nCoV pseudovirus trapping, after the laser is switched on at 34.90 s, the virus is trapped towards the laser spot center. c) Trapping and manipulation of an *E. coli* cell through a "PS gate", where two printed PSs (1 μm in diameter) are located on the Au film as reference. d) Fabricating a nano PS-star by combining a larger PS (1 μm) and a smaller PS (500 nm) with opposite surface charges. e) The transport and immobilization of AuNS-50 nm onto the target *E. coli* cell. The PEG mass fraction in (a,c,d) and (b) is 5% and 10%, respectively. The red dashed circles and arrows indicate that the laser spot and the manipulation trajectory. The video frames in (a,b,e) and (c,d) were recorded by dark-field and bright-field microscopy, respectively. The optical power of 785 nm laser is 0.3 mW.

directly on the AuNS via particle-polymer boundary interaction to drive the particle.[43,44] In our experiments, 3.3 nm AuNSs cannot be firmly trapped in a PEG-5% solution, but they can be trapped effectively in a PEG-10% solution. We attribute this phenomenon to the PEG chain's mesh size ξ (depicted in Figure 1e). When the AuNS diameter is smaller than ξ, effective trapping becomes challenging. Conversely, if the diameter exceeds ξ, the AuNS becomes more prone to be trapped due to increased interaction between PEG chains and the AuNS boundary.

The HAONT scheme is suitable for trapping and manipulating a wide range of nanoparticles composed of organics and inorganics. First, the trapping of polystyrene spheres (PSs) is tested. As the video frames in **Figure 2**a indicate, we have achieved the dynamic trapping and releasing of multiple PSs of 200 nm in diameter (see Video S1, Supporting Information). In addition, the trapping and manipulation of PSs of sizes ranging from 100 to 1000 nm is also achieved. Note that the operation laser spot is loosely focused to a radius (R_s) of about 500 nm. The optical power (measured after the objective) required for trapping PS is in the range of 5 μW–1 mW, which corresponds to a minimum power density of about 6.4 μW μm^{-2}.

HAONT is also good for bio-nanoparticle trapping. For example, as shown in Figure 2c,d, we have successfully trapped a single inactivated pseudovirus of 2019-nCoV (Zoonbio Biotechnology Inc.). A video of the full event is shown in Video S2, Supporting Information. Moreover, an *E. coli* cell can also be readily trapped and manipulated for traveling through a "PS gate" (see Video S3, Supporting Information). In addition, the trapping ability of HAONT for exosomes-HEK is also verified. It is worth noting that the effective trapping conditions for bio-nanoparticles are size-dependent, much like their non-metal counterparts, such as polystyrene (PS) as depicted in Figure 1d. Micro-sized particles, such as *E. coli* cells, can be trapped at PEG mass fractions above 1%. In contrast, nano-sized particles like pseudovirus or exosomes (≈100 nm) require a PEG mass fraction greater than 5% for effective trapping.

Clearly, with more experimental trials, we are highly optimistic that the reported HAONT scheme has a high potential for more versatile bio-nanoparticle manipulation operations.

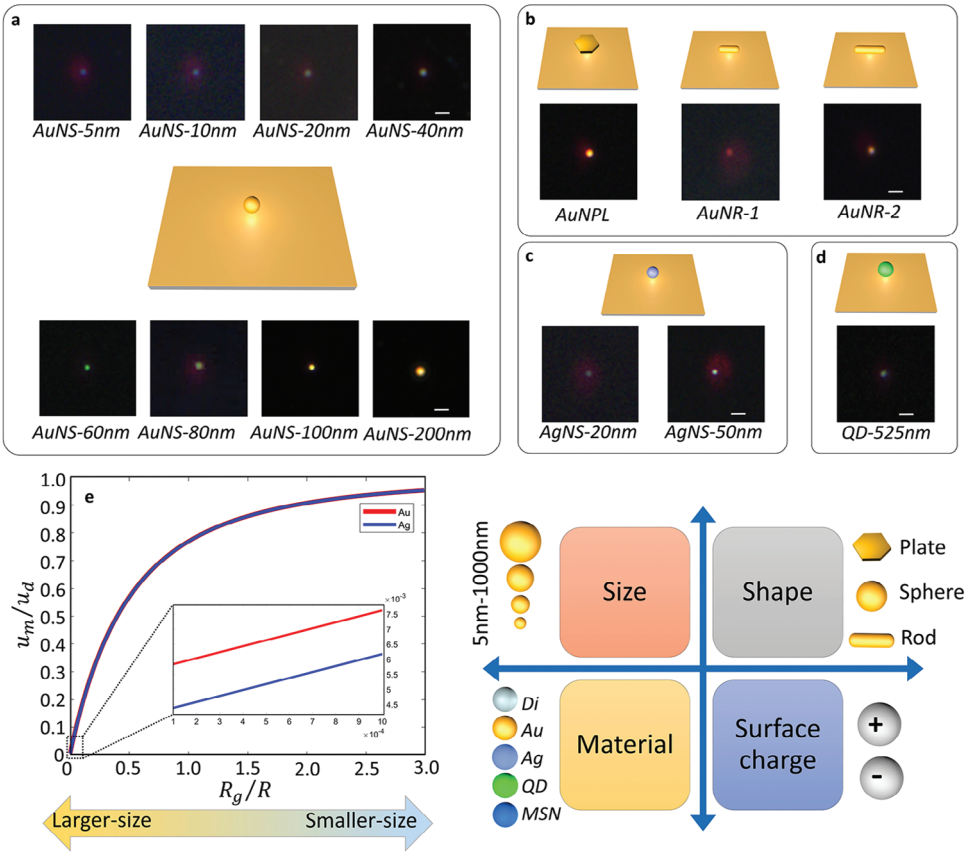

Figure 3. Single inorganic nanoparticle trapping of different materials, surface charges, sizes, and shapes. a) Trapping of gold nanospheres (AuNSs) with diameters ranging from 5 to 200 nm. b) Trapping of Hexagonal Au nanoplate (H-AuNPL), two kinds of gold nanorods (AuNR-1/2). c) Trapping of silver nanosphere (AgNS) with diameters of 20 and 50 nm. d) Trapping of a quantum dot with 525 nm emission wavelength (QD-525 nm). The detail of the nanoparticle's preparation is shown in the Experimental Section. The optical power of 785 nm laser is 0.5 mW, and the images were recorded by dark-field microscopy. e) The relationship between the velocity ratio (u_m/u_d) and the metal particle radius ratio (R_g/R). Two curves of gold (Au) and silver (Ag) material are presented. The inset indicates the case for larger metal particles. The thermal conductivity of Au and Ag is 318 and 429 W m^{-1} K^{-1}, respectively, and the solution is water (κ_s= 0.6 W m^{-1} K^{-1}). Di indicates dielectric particles such as PS and bio-nanoparticles.

Furthermore, metal nanoparticles are relatively un-susceptible to the temperature gradient because of their temperature field homogenization effect. As shown in **Figure 3**, we successfully trapped individual gold nanospheres (AuNSs) and silver nanospheres (AgNSs) spanning sizes of 5 to 200 nm. Additionally, we tested the trapping of gold nanoparticles in various shapes, including gold nanorods (AuNRs) and hexagonal gold nanoplate (H-AuNPL). In our experiments, a water-based solution with relatively low salinity was employed. Consequently, based on DLVO theory, the direct trapping and printing of target particles on the substrate was rarely observed.[35] However, during extended trapping durations (e.g., 20 min), nanoparticles would occasionally settle and adhere to the substrate. To further verify the trapping event, we did the in situ SEM imaging of these trapped and printed nanoparticles (see Note S8, Supporting Information). Moreover, semiconductor materials such as quantum dots (QDs) and mesoporous silica nanoparticles (MSNs) can also be trapped. Details of nanoparticle preparation procedures are presented in Note S9, Supporting Information. In addition, because of temperature homogenization induced by the metal nanoparticles, the minimum optical power required for metal nanoparticle trapping is much larger, which is about 80 μW, that is, 102 μW μm^{-2} in power density. Nevertheless, the overall trapping power density required of HAONT is quite low, which is about a third order of magnitude smaller than the classic optical tweezers (10–100 mW μm^{-2}). And the heating effect of the metal nanoparticle itself is negligible at such low power intensities according to previous comprehensive studies of plasmonic heating in nanoparticles.[71,72]

Furthermore, the HAONT can also trap particles with varying surface charges. The aforementioned metal nanoparticles and PSs exhibit distinct surface charges in both positive and negative ranges. Notably, the surface charges of different nanoparticles remain nearly constant across different PEG mass fractions (refer to Note S3, Supporting Information). This has made HAONT a good candidate for adopting a wider range of nano-fabrication and biological applications. As shown in Figure 2d, we successfully assembled a PS-star structure using PS particles of different surface functionalizations. By mixing amino-functionalized larger PS particles (1 μm) and carboxyl-functionalized smaller PS particles (500 nm) in the microfluidic chamber, larger particles deposit onto the Au film.

Subsequently, we captured multiple smaller PS particles and transported them to the surface of the larger PS, resulting in instantaneous binding through dehydration condensation. This process leads to the formation of a "nano PS-star" structure (refer to Video S4, Supporting Information). Moreover, the plasmonic gold nanoparticle-based nano-probes have contributed a lot to biological study.[73–76] However, achieving precise simultaneous manipulation across microscale bioparticles and nanoparticles remains challenging. HAONT can also promote the interactions between cells and AuNS and gather them into a biocompatible assembly. As depicted in Figure 2e, we perform AuNS-50 nm cluster trapping and transport towards the target *E. coli* cell (see Video S5, Supporting Information), allowing for the immobilization of AuNS onto the target cell via bacteria surface sorption. This further enhances HAONT's versatility for various biocompatible nano-manipulation tasks.

2.3. Trapping Stiffness-Based Nanoparticles Sorting

In the HAONT scheme, the dominant thermodynamic forces exerted on the target particles can be calculated via Stokes' law $F = 6\pi\eta Ru$, where R is the radius of the trapped particles and u the relative velocity between the particle and the fluid. In the case of common dielectric particles that have a similar or smaller thermal conductivity (κ_p) compared to the surrounding solution (κ_s), the nanoparticle will not homogenize the temperature gradient ∇T around it. Therefore, the trapping stiffness increases linearly with R and u. However, metal nanoparticles normally have larger thermal conductivity, which will in turn decrease the ∇T around them, and lead to a lower trapping stiffness because of this temperature field homogenization effect.

To explore the size-dependency nature of this metal-nanoparticle-induced ∇T homogenization effect, we compared the optothermal-driven velocity of a metal particle (u_m), which possesses higher thermal conductivity than the surrounding solution, to its dielectric counterpart of the same size (u_d), which exhibits thermal conductivity similar to that of the solution. As shown in Figure 3e, we plot the curve of the velocity ratio (u_m/u_d) corresponding to the metal particle radius (see Note S6, Supporting Information for details). It indicates that for larger-sized metal nanoparticles (e.g., AuNS of 200–100 nm), the ∇T homogenization effect is much more remarkable ($u_m/u_d \ll 1$) than the smaller-sized metal nanoparticles (e.g., AuNS of 5–20 nm). And the difference between Au and Ag is non-significant.

Subsequently, we measured the trapping stiffness of AuNS and PS and the experimental results were consistent with our theoretical analysis. As shown in **Figure 4**a–f, the trapping stiffness of nanoparticles is affected by size, material, and PEG concentration. A higher PEG mass fraction or larger particle size results in increased trapping stiffness. This occurs because larger particles with greater surface area are more influenced by diffusiophoresis forces from surrounding PEG molecules. As the correlation length ξ decreases, a denser PEG network forms around the particle, leading to stronger diffusiophoresis forces (see Figure 1e). Thus, when the ratio of particle radius (R) to correlation length (ξ), that is, R/ξ, increases, diffusiophoretic forces become more significant.[43,44] Additionally, due to the temperature homogenization effect, the trapping stiffness of AuNS-200 and 100 nm becomes comparable, while the trapping stiffness of PS-200 nm is ≈2.5 times greater than that of AuNS-200 nm.

Counterintuitively, we observed a tendency for the trapping stiffness to plateau as the laser power gradually increases. Further increments in laser power result in higher local temperatures, which results in a reduction in trapping stiffness (also demonstrated by the relative trapping stiffness normalized by power in Figure S13, Supporting Information). This is because, with an increase in temperature, the absolute value of $D_T + D_T^{PEG}$ decreases, while the thermo-osmotic flow (χ) concurrently intensifies (details explained in Note S7, Supporting Information). Furthermore, at higher laser power levels (> 0.6 mW), this phenomenon also leads to an intriguing doughnut-shaped vortex (DSV) trapping behavior, as elaborated in the following sections (**Figure 5**).

Additionally, by driving particles through the solution at varying velocities, sorting can be achieved between larger and smaller particles based on the disparities in their trapping stiffness. Remarkably, sorting can also be achieved between different materials, for instance, by isolating PS particles from a mixed solution of AuNS-200 and PS-200 nm, which demonstrates the capacity to selectively trap and sort specific particles even within a nanoparticle mixture of the same size. As shown in Video S6, Supporting Information and Figure 4g, when the heating laser captures two distinct nanospheres and brings them close, moving them at a higher speed results in the release and separation of AuNS-200 nm while retaining and sorting out the PS-200 nm within the trapping potential well. Hence, the HAONT approach demonstrates a versatile capability for nanoparticle sorting based on both size and material.

To get a quantitative view of the particle confinement ability of HAONT, as depicted in **Figure 6**, we conducted a numerical simulation on the thermodynamic force distribution based on Stokes' law along with the consideration of temperature field homogenization. Figure 6a–c shows that the diffusiophoretic force (F_D) facilitates the trapping of the nanoparticle along ∇T, directing it towards the hotter center. Meanwhile, the role of thermo-osmotic force (F_{TO}) in trapping is mainly to assist particles in being trapped along the x/y directions parallel to the substrate. While its upward component (positive z-direction) of thermo-osmotic flow at the center of capture near the substrate is unfavorable for particle trapping. Nevertheless, the diffusiophoretic force in the negative z-direction compensates for this repelling contribution, ultimately leading to successful trapping. We also calculated the optical forces using dipole approximation by considering the complex polarizability correction term.[77,78] It indicates that the optical force (F_O) is about one order of magnitude smaller than the dominated thermodynamic forces (F_D, F_{TO}) in this trapping scheme (Figure 6g). We also conducted controlled trapping experiments for nanoparticles without the gold film deposition and observed that it was challenging to trap the particles under such lower laser power conditions(< 0.62 mW). The simulation shows that particles of the same material exhibit larger trapping forces with increasing size. Moreover, when comparing net trapping forces for AuNS and PS particles of the same size (200 nm), due to gold nanoparticles' higher thermal conductivity, PS exhibits significantly higher net force and deeper trapping potential than AuNS (Figure 6d–f). This observation aligns with

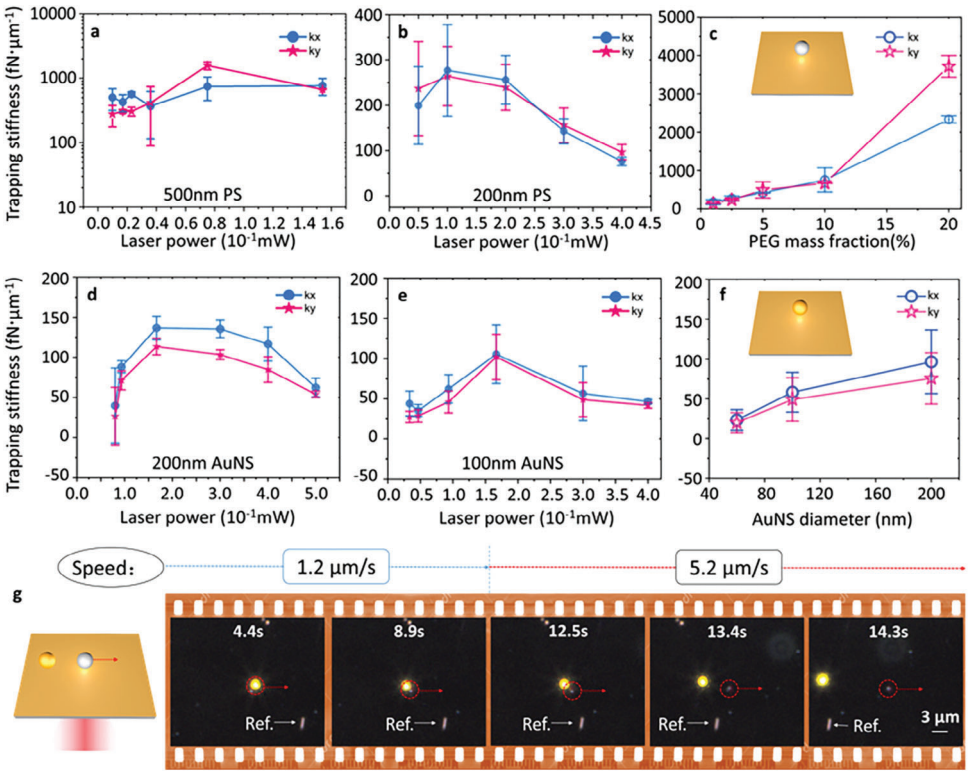

Figure 4. Trapping stiffness measurements of different PEG mass fractions and nanoparticle sizes. a,b) Trapping stiffness values of single PS at different laser power levels at a PEG mass fraction of 10%, and the PS diameters are a) 500 and b) 200 nm. c) Trapping stiffness values of single PS-500 nm in different PEG mass fractions, optical power is 0.13 mW. d,e) Trapping stiffness values of single AuNS in different laser powers at PEG mass fraction of 10%, the AuNS diameters are d) 200 and e) 100 nm. Each data point in (a–c) is an average of three independent measurements. f) Trapping stiffness values of single AuNS in different sizes, each data point is an average value of the trapping stiffness measured at different laser powers. More trapping stiffness measurement data are presented in Note S10, Supporting Information. g) The AuNS-200 and PS-200 nm move together at a low heating laser translocation speed of 1.2 μm $^{-1}$s, while after increasing the speed to 5.2 μm $^{-1}$s, PS-200 nm remained in the trap and was sorted out from the AuNS-200 nm.

experimental trapping stiffness data displayed in Figure 4b,d. Additionally, we analyze the in plane force distribution (Figure S11, Supporting Information) and its *z*-component ($F_{Net}(z)$) (Figure 6i) for AuNSs of varying sizes. Due to the positive $F_{Net}(z)$, larger trapped particles (2R > 50 nm) exhibit a tendency to be captured from the radial direction. Furthermore, relying on force simulations in Figure 6f, we computed corresponding trapping stiffness values, which exhibit good agreement with measurements across various nanoparticles (see Note S10, and Table S1, Supporting Information). Therefore, our theoretical and experimental studies have given a comprehensive understanding of the HAONT's versatile and highly adaptable particle manipulation ability.

2.4. Doughnut-Shaped Vortex Trapping and Biological Applications

Remarkably, due to the amplified thermo-osmotic flow and the diminished diffusiophoresis coefficient at elevated temperatures under higher laser powers (also refers to Note S7, Supporting Information), as depicted in **Figure 5**a, increasing the laser power to 0.6 mW results in the creation of an intriguing trapping configuration: a doughnut-shaped vortex (DSV) trapping scheme in which particles are trapped and circulate around the laser spot. The diameter of the DSV trapping region for AuNS-50 nm expands as the laser power increases (see Figure 5b and Video S7, Supporting Information). Moreover, in conventional MSN-based drug delivery, nanoparticles typically approach cell surfaces through passive Brownian motion, resulting in limited cell targeting precision.[79] However, HAONT offers an opportunity to enhance drug delivery accuracy and efficiency, transforming passive diffusion into an active process. As depicted in Figure 5c, at a laser power of 0.62 mW, the MSNs with diameters of ≈100 nm (for preparation details, please refer to Note S9, Supporting Information) can also be induced into a DSV trapping mode, allowing them to follow the movement of the laser spot (see Video S8, Supporting Information). Additionally, unlike smaller nanoparticles trapped within the doughnut-shaped vortex zone influenced by thermo-osmotic flow, larger cells with greater gravity force tend to be captured at the center under the same laser power. As shown in Figure 5d, we can guide the target *E. coli* cell to the center of the DSV trap (see Video S9, Supporting Information). This not only significantly enhances interaction probability and accuracy, but also introduces a novel physical interaction mode between the cell and the MSN.

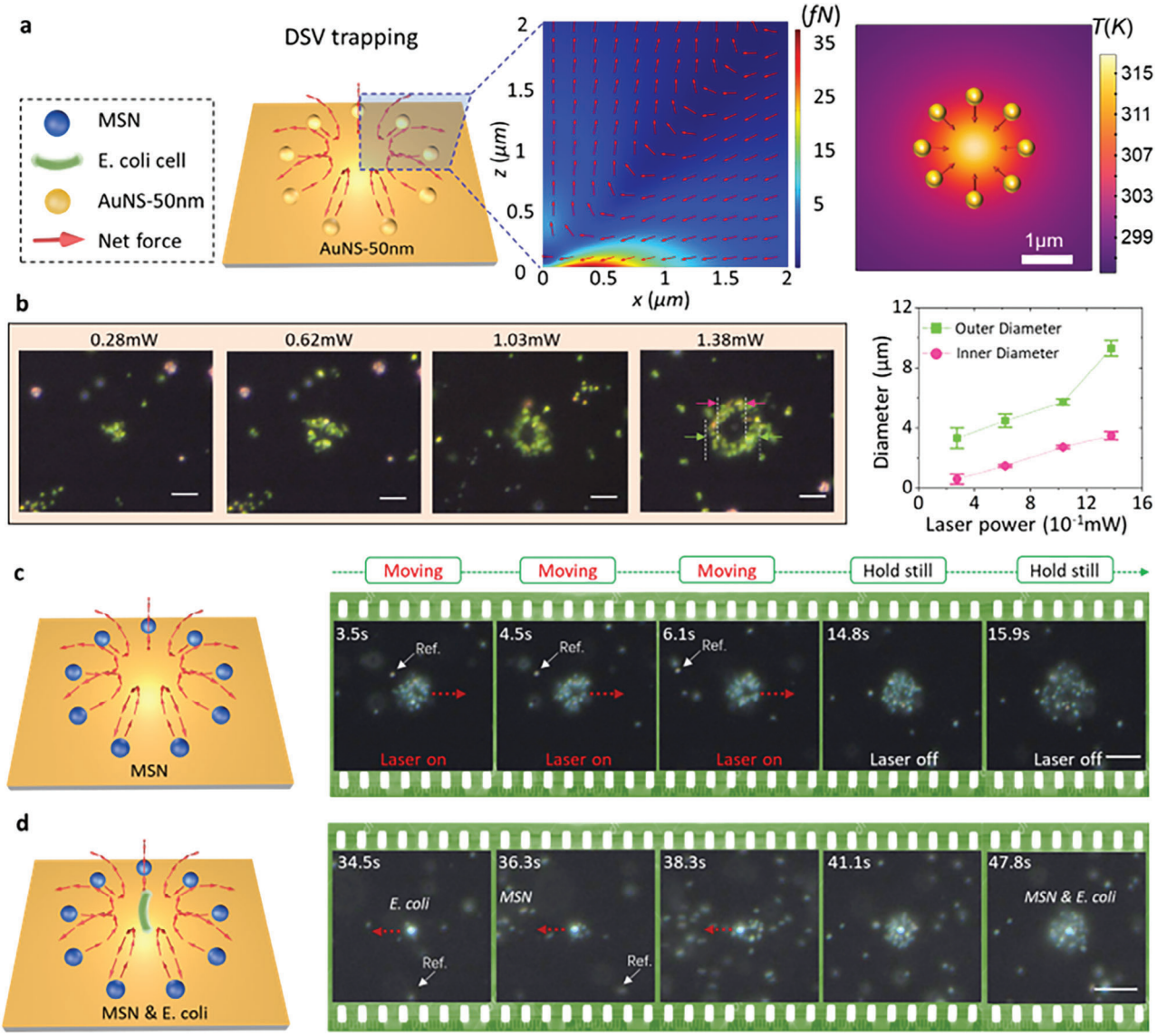

Figure 5. Doughnut-shaped vortex (DSV) nanoparticle manipulation and interactions with *E. coli* cells. a) The DSV trapping mode of an AuNS-50 nm cluster with insets displaying net force distribution in the *x*–*z* plane and temperature distribution in the *x*–*y* plane, the laser power is 0.6 mW. b) The DSV trapping mode of an AuNS-50 nm cluster at different laser powers, and the relationship between the inner/outer diameter of the doughnut-shaped trapping region and the laser power. c) The DSV trapping mode and the movement of a mesoporous silica nanoparticle (MSN) cluster. d) The DSV trapping process of an MSN cluster around an *E. coli* cell. The length of the scale bars in (b–e) is 5 μm.

Therefore, the versatile manipulation capabilities of HAONT, spanning nanoscale to microscale and across different biological species, make it a valuable tool for diverse applications. For instance, the precise interaction between MSNs and cells holds the potential for accurate single-cell drug delivery. Immobilizing metal nanoparticles on bacterial surfaces, such as *E. coli* cells, enables in situ surface-enhanced Raman scattering (SERS) applications for detecting biological differences at a sub-cellular level,[80] inter-bacteria communications,[76] or antibacterial applications. Moreover, HAONT facilitates the manipulation of DNA or RNA molecules through diffusiophoresis,[49] allowing for simultaneous trapping and bioreactions. The optothermal effect also provides favorable temperature conditions for various biochemical reactions, including polymerase chain reaction (PCR), DNA hybridization, or enzymatic reactions.

3. Conclusion

In this study, through innovatively incorporating the diffusiophoresis and thermo-osmotic flows in the boundary layer of an optothermal responsive Au film, we have demonstrated a novel nano-manipulation technique entitled HAONT. It is a universal manipulation tool with low operating power, single-particle resolution, and biocompatible character. It also introduced a novel physical tweezering mode of DSV trapping, which facilitates new interactions between nanoparticles and cells. HAONT is highly

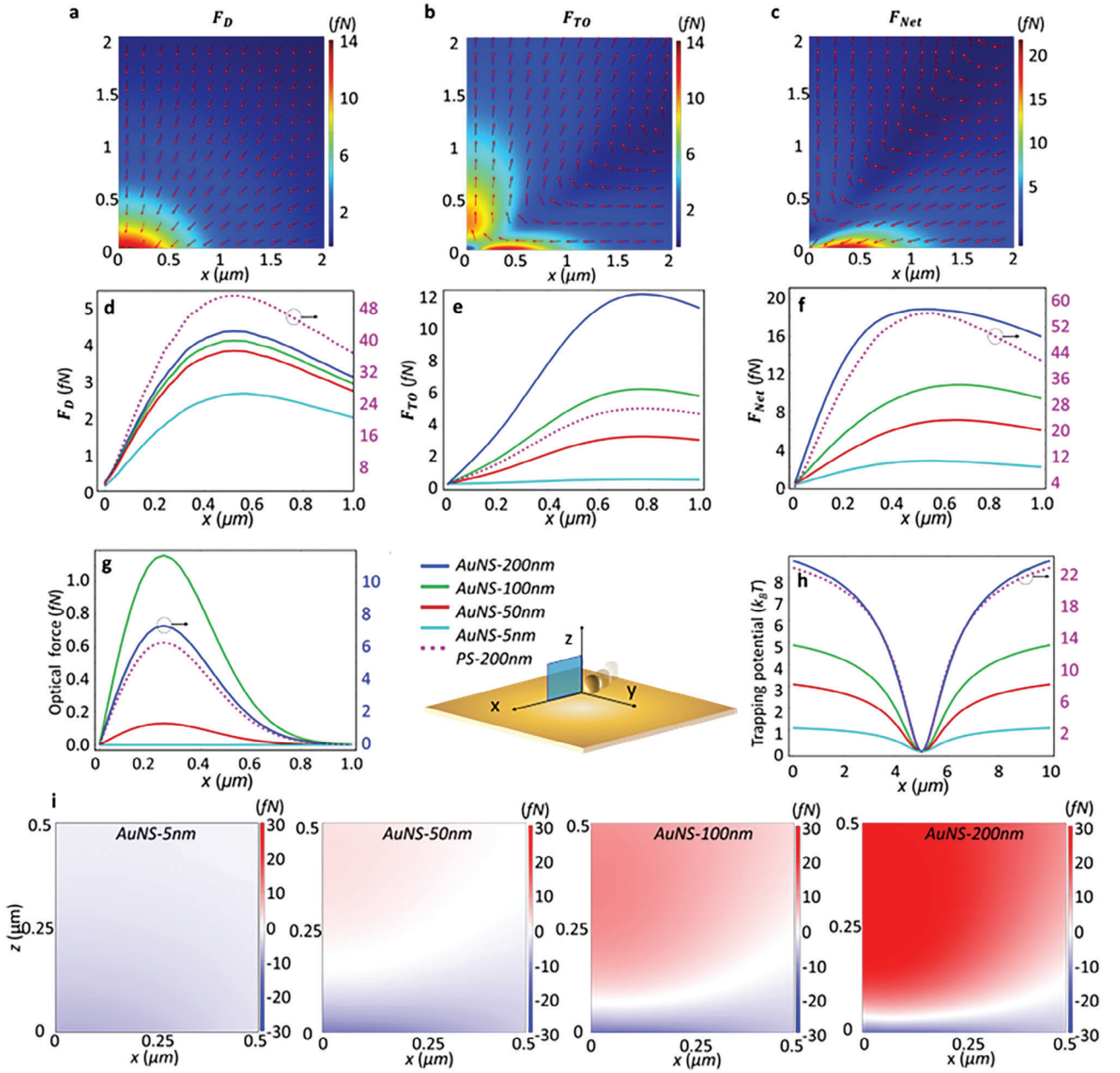

Figure 6. Forces in the HAONT. a–c) In plane spatial distribution of the diffusiophoretic force (F_D), thermo-osmotic force (F_{TO}), and net force (F_{Net}) respectively for an AuNS-50 nm. d–f) Radial force variation of F_D, F_{TO}, and F_{Net} respectively. g) Radial force variation of the optical force (F_O). h) The trapping potential of different particles. i) In plane force distribution of the *z*-component of the net force ($F_{Net}(z)$) of different AuNSs, negative means the force is in the *z*-direction. The analyzing particles are AuNSs of different sizes and PS (200 nm). The heating laser spot center is located at (0, 0), and the radial force variation is measured at 100 nm above the Au film substrate. The optical power of the 785 nm laser is 0.3 mW and the PEG mass fraction is 10%.

customizable for the manipulation of a wide range of nanoparticles of different sizes, shapes, materials, and biological forms without surface modification. By tuning suitable optical power and PEG concentration, one can perform as-demand and precise nanostructure trapping and assembling tasks. Traditionally, metal nanoparticles pose a challenge for traditional optothermal tweezers due to two factors. Firstly, their enhanced optical scattering force hinders stable trapping when their sizes are similar to the laser wavelength.[81,82] Secondly, metal nanoparticles with high thermal conductivity are less affected by temperature gradients due to their temperature homogenization effect. Nonetheless, HAONT has demonstrated successful trapping of metal nanoparticles including gold and silver, spanning diameters from 5 to 200 nm. Moreover, we conducted a comprehensive study of the optical and thermodynamic forces in the HAONT scheme, alongside an examination of its trapping stiffness. The outcomes

affirm the scheme's capability for sorting nanoparticles based on their material and size. Additionally, the HAONT can operate effectively in common biomedical buffer solutions like TRIS hydrochloride.

However, HAONT also has limitations. Firstly, unlike conventional optical tweezers that allow accurate measurement of external forces,[6,83] HAONT requires Stokes' drag force for potential measurement. Moreover, the changing viscosity due to the concentration gradient of polymers impacts its accuracy. Secondly, HAONT intrinsically relies on particle-solution boundary interactions, the trapping stiffness is relatively low, and it is challenging to trap single non-rigid nanoparticles with soft morphologies like short single-strand nucleic acid or proteins. Thirdly, accomplishing 3D manipulation is unfeasible due to the trapping scheme's reliance on a planar thermal-responsive substrate. Moreover, in terms of thermal impact on biological samples, we recommend that researchers first determine the maximum temperature tolerance of the specific samples they are working with. Subsequently, to maintain the viability, they can refer to Figure S1 and Note S1, Supporting Information and select an appropriate laser power that ensures the temperature remains below this threshold, for example, less than 0.3 mW(< 35 °C), which aligns well with the conditions for a wide range of biological samples such as virus, cells, or exosomes, as most of them are cultured at 37 °C incubator.[84,85] While HAONT works well for some thermoresistant cells like *E. coli*, capable of surviving temperatures as high as 50 °C.[86,87] This implies that they can also survive under the conditions of DSV mode, which reaches a maximum temperature of 42 °C (0.6 mW). Despite its current limitations, we believe that with further refinements, such as integrating temperature control technique[56] or introducing electronic fields,[14–16] the inherent biocompatibility and adaptability of the HAONT scheme will enable it to become a versatile nano-manipulation tool suitable for various applications in synthetic biology, colloidal science, nanotechnology, and biomedical research.

4. Experimental Section

Optical Setup: The optical setup was based on a Nikon inverted microscope (Ti2-E), with a 785 nm solid-state laser that was expanded (5×) and reflected by a non-polarizing plate beam splitter (R: T = 90:10, 700–1100 nm, Thorlabs). A 100× oil dark-field objective (Nikon, NA = 1.3) was used to focus the laser onto the optothermal substrate. The beam expansion system was adjusted to achieve a loosely focused laser spot, with a diameter of 1 µm, to ensure compatibility with the image recording optical setup. Optical images were captured using a colored sCMOS camera (Dhyana 400DC, Tucsen Ltd.). To block the reflected 785 nm laser, a short pass filter (OD = 4, cut-off wavelength = 675 nm, Edmund) was utilized. Dark-field oil condenser (Nikon, NA = 1.43–1.20) and bright-field condenser were employed for sample illumination.

Material Preparation: The optothermal substrate (Au film) was prepared by depositing an Au thin layer (10 nm) on a coverglass slide (20 × 20 mm). An adhesion layer of chromium (5 nm) was deposited prior to the gold film deposition. The deposition procedures were provided by Suzhou Hengxin Microelectronics CO., Ltd. The microfluidic chip was composed of a glass slide (76 × 26 mm) and Au film deposited the coverglass slide, in which they were sealed and separated by a thin layer of parafilm. The height of the microfluidic chip was ≈30 µm. The procedures for synthesizing the Au nanoparticles (3.3 and 5–20 nm), MSN, and procedures of exosome extraction are shown in Note S8, Supporting Information. The gold nanorods (AuNR-1, 20 × 40 nm, absorption peak: 610 ± 10 nm; AuNR-2, 25 × 80 nm, absorption peak: 720 ± 10 nm) and silver nanospheres (AgNSs) were purchased from Zhongke Leiming Technology CO., Ltd. The 15 nm AuNS was purchased from Nanoeast Biotech CO., Ltd. The AuNSs (40–200 nm) and Au nanoplate (AuNPL) were purchased from NanoSeedz CO., Ltd. The polystyrene beads were purchased from Bangs Laboratories CO., Ltd. Fluorescent QDs (emission wavelength: 525 nm) were purchased from Aladdin CO., Ltd.

Trapping Stiffness Measurement: Trapping stiffness was determined through the equipartition method[88] and analyzed using a high-speed grayscale CMOS camera (Imaging Source Ltd.) at an imaging speed of 500 fps. An optical trap calibration method was adopted to obtain accurate results.[89] The centroid method was employed to identify particle center positions, enabling the extraction of particle position distribution from grayscale images. The optical setup used was consistent with the HAONT experiments. In addition, due to the extended integration time required for microscopic observation of smaller AuNS-5 nm, as well as its inherently weaker trapping stiffness, employing the equipartition method, which was used for most larger particles, became challenging. Instead, the trapping stiffness of AuNS-5 nm was determined using the drag force method.[1,90]

Finite Elements Method Simulations: A commercialized simulation software of COMSOL Multiphysics was used to calculate the temperature distribution and force distribution around the optothermal substrate. A 2D-axisymmetric geometry model composed of a gold film, glass substrate, and solvent was built. An optothermal heat source with a Gaussian profile was set at the interface of the gold film and the solvent. Heat transfer and laminar flow models in fluids were used to calculate the thermophoresis and thermos-osmotic flow field. Room temperature was set as 25 °C at all other boundaries except for the optothermal heat source. Moreover, accounting for the depletion of PEG molecules from the trapping center (PEG concentration $c(r) = c_0 e^{-S_T^m \Delta T(r)}$), the viscosity of the solution (10% PEG) was established within the simulated region as 2.57 × 10^{-3} Pa s, aligning with the viscosity of 5% PEG solution.[62] This viscosity approximation remained reasonable in proximity to the trapping center. In addition, to calculate the optical force, the electromagnetic wave model was used in the frequency domain, dipole approximation was adopted for obtaining optical gradient force, and scattering force was exerted on the nanoparticles.[77]

Supporting Information

Supporting Information is available from the Wiley Online Library or from the author.

Acknowledgements

This work was supported by the National Natural Science Foundation of China (62275164, 61905145, 62275168, 61775148); National Key Research and Development Program of China (No. 2022YFA1206300); Guangdong Natural Science Foundation and Province Project (2021A1515011916, 2023A1515012250); Foundation from Department of Science and Technology of Guangdong Province (2021QN02Y124); Shenzhen Science and Technology R&D and Innovation Foundation (JCYJ20200109105608771); Shenzhen Science and Technology Planning Project (ZDSYS20210623092006020); Medical-Engineering Interdisciplinary Research Foundation of Shenzhen University (2023YG002).

Conflict of Interest

The authors declare no conflict of interest.

Data Availability Statement

The data that support the findings of this study are available from the corresponding author upon reasonable request.

Keywords

assembling, diffusiophoresis, nanostructure fabrication, optical tweezers, optothermal trapping, thermo-osmosis

Received: September 6, 2023
Revised: October 28, 2023
Published online: December 14, 2023

[1] A. Ashkin, J. M. Dziedzic, J. E. Bjorkholm, S. Chu, *Opt. Lett.* **1986**, *11*, 288.
[2] R.-J. Essiambre, *Proc. Natl. Acad. Sci. U. S. A.* **2021**, *118*, 2026827118.
[3] T. Pan, D. Lu, H. Xin, B. Li, *Light: Sci. Appl.* **2021**, *10*, 124.
[4] H. Xin, Y. Li, Y.-C. Liu, Y. Zhang, Y.-F. Xiao, B. Li, *Adv. Mater.* **2020**, *32*, 2001994.
[5] Y. Shi, X. Xu, M. Nieto-Vesperinas, Q. Song, A. Q. Liu, G. Cipparrone, Z. Su, B. Yao, Z. Wang, C.-W. Qiu, X. Cheng, *Adv. Opt. Photonics* **2023**, *15*, 835.
[6] P. M. Hansen, V. K. Bhatia, N. Harrit, L. Oddershede, *Nano Lett.* **2005**, *5*, 1937.
[7] F. Hajizadeh, S. N. S. Reihani, *Opt. Express* **2010**, *18*, 551.
[8] P. M. Bendix, L. Jauffred, K. Norregaard, L. B. Oddershede, *IEEE J. Sel. Top. Quantum Electron.* **2013**, *20*, 15.
[9] P. M. Bendix, L. B. Oddershede, *Nano Lett.* **2011**, *11*, 5431.
[10] H. Luo, X. Fang, C. Li, X. Dai, N. Ru, M. You, T. He, P. C. Wu, Z. Wang, Y. Shi, X. Cheng, *Small Sci.* **2023**, *3*, 2300100.
[11] F. Nan, F. J. Rodríguez-Fortuño, S. Yan, J. J. Kingsley-Smith, J. Ng, B. Yao, Z. Yan, X. Xu, *Nat. Commun.* **2023**, *14*, 6361.
[12] M. L. Juan, M. Righini, R. Quidant, *Nat. Photonics* **2011**, *5*, 349.
[13] Y. Shi, Q. Song, I. Toftul, T. Zhu, Y. Yu, W. Zhu, D. P. Tsai, Y. Kivshar, A. Q. Liu, *Appl. Phys. Rev.* **2022**, *9*, 031303.
[14] M. C. Wu, *Nat. Photonics* **2011**, *5*, 322.
[15] S. Zhang, B. Xu, M. Elsayed, F. Nan, W. Liang, J. K. Valley, L. Liu, Q. Huang, M. C. Wu, A. R. Wheeler, *Chem. Soc. Rev.* **2022**, *51*, 9203.
[16] X. Chen, X. Chen, M. Elsayed, H. Edwards, J. Liu, Y. Peng, H. P. Zhang, S. Zhang, W. Wang, A. R. Wheeler, *ACS Nano* **2023**, *17*, 5894.
[17] S. Zhang, M. Elsayed, R. Peng, Y. Chen, Y. Zhang, J. Peng, W. Li, M. D. Chamberlain, A. Nikitina, S. Yu, X. Liu, S. L. Neale, A. R. Wheeler, *Nat. Commun.* **2021**, *12*, 5349.
[18] S. Zhang, W. Li, M. Elsayed, J. Peng, Y. Chen, Y. Zhang, Y. Zhang, M. Shayegannia, W. Dou, T. Wang, Y. Sun, N. P. Kherani, S. L. Neale, A. R. Wheeler, *Small* **2021**, *17*, 2103702.
[19] Y. Zhu, M. You, Y. Shi, H. Huang, Z. Wei, T. He, S. Xiong, Z. Wang, X. Cheng, *Micromachines* **2023**, *14*, 1326.
[20] Y. Shi, Y. Wu, L. K. Chin, Z. Li, J. Liu, M. K. Chen, S. Wang, Y. Zhang, P. Y. Liu, X. Zhou, *Laser Photonics Rev.* **2022**, *16*, 2100197.
[21] I. D. Stoev, B. Seelbinder, E. Erben, N. Maghelli, M. Kreysing, *eLight* **2021**, *1*, 7.
[22] Y. Shi, K. T. Nguyen, L. K. Chin, Z. Li, L. Xiao, H. Cai, R. Yu, W. Huang, S. Feng, P. H. Yap, J. Liu, Y. Zhang, A. Q. Liu, *ACS Sens.* **2021**, *6*, 3445.
[23] F. Nan, Z. Yan, *Nano Lett.* **2018**, *18*, 7400.
[24] Y. Liu, H. Ding, J. Li, X. Lou, M. Yang, Y. Zheng, *eLight* **2022**, *2*, 13.
[25] A. Minopoli, S. Wagner, E. Erben, W. Liao, I. D. Stoev, E. Lauga, M. Kreysing, *eLight* **2023**, *3*, 16.
[26] L. Lin, E. H. Hill, X. Peng, Y. Zheng, *Acc. Chem. Res.* **2018**, *51*, 1465.
[27] J. Chen, J. F.-C. Loo, D. Wang, Y. Zhang, S.-K. Kong, H.-P. Ho, *Adv. Opt. Mater.* **2020**, *8*, 1900829.
[28] Y. Pang, R. Gordon, *Nano Lett.* **2012**, *12*, 402.
[29] Y. Liu, A. W. Poon, *Opt. Express* **2010**, *18*, 18483.
[30] M. Braun, F. Cichos, *ACS Nano* **2013**, *7*, 11200.
[31] Z. Kang, J. Chen, S.-Y. Wu, K. Chen, S.-K. Kong, K.-T. Yong, H.-P. Ho, *Sci. Rep.* **2015**, *5*, 9978.
[32] L. Lin, M. Wang, X. Peng, E. N. Lissek, Z. Mao, L. Scarabelli, E. Adkins, S. Coskun, H. E. Unalan, B. A. Korgel, L. M. Liz-Marzán, E.-L. Florin, Y. Zheng, *Nat. Photonics* **2018**, *12*, 195.
[33] H. Cong, J. Chen, H.-P. Ho, *Sens. Actuators, B* **2018**, *264*, 224.
[34] H. Cong, J. Loo, J. Chen, Y. Wang, S.-K. Kong, H.-P. Ho, *Biosens. Bioelectron.* **2019**, *133*, 236.
[35] M. Fränzl, F. Cichos, *Nat. Commun.* **2022**, *13*, 656.
[36] J. Chen, Y. Zeng, J. Zhou, X. Wang, B. Jia, R. Miyan, T. Zhang, W. Sang, Y. Wang, H. Qiu, J. Qu, H.-P. Ho, B. Z. Gao, Y. Shao, Y. Gu, *Biosens. Bioelectron.* **2022**, *204*, 114084.
[37] X. Wang, Y. Yuan, X. Xie, Y. Zhang, C. Min, X. Yuan, *Adv. Mater.* **2022**, *34*, 2107691.
[38] J. Chen, Z. Kang, S. K. Kong, H.-P. Ho, *Opt. Lett.* **2015**, *40*, 3926.
[39] J. Chen, H. Cong, F.-C. Loo, Z. Kang, M. Tang, H. Zhang, S.-Y. Wu, S.-K. Kong, H.-P. Ho, *Sci. Rep.* **2016**, *6*, 35814.
[40] L. Lin, X. Peng, Z. Mao, X. Wei, C. Xie, Y. Zheng, *Lab Chip* **2017**, *17*, 3061.
[41] H. Ding, P. S. Kollipara, L. Lin, Y. Zheng, *Nano Res.* **2021**, *14*, 295.
[42] Q. Jiang, B. Rogez, J.-B. Claude, G. Baffou, J. Wenger, *Nano Lett.* **2020**, *20*, 8811.
[43] A. Würger, *Rep. Prog. Phys.* **2010**, *73*, 126601.
[44] J. L. Anderson, *Annu. Rev. Fluid Mech.* **1989**, *21*, 61.
[45] M. Reichl, M. Herzog, F. Greiss, M. Wolff, D. Braun, *Phys. Rev. E* **2015**, *91*, 062709.
[46] D. Braun, A. Libchaber, *Phys. Rev. Lett.* **2002**, *89*, 188103.
[47] H.-R. Jiang, H. Wada, N. Yoshinaga, M. Sano, *Phys. Rev. Lett.* **2009**, *102*, 208301.
[48] Y. T. Maeda, *Appl. Phys. Lett.* **2013**, *103*, 243704.
[49] Y. T. Maeda, T. Tlusty, A. Libchaber, *Proc. Natl. Acad. Sci. USA* **2012**, *109*, 17972.
[50] H. Ding, Z. Chen, P. S. Kollipara, Y. Liu, Y. Kim, S. Huang, Y. Zheng, *ACS Nano* **2022**, *16*, 10878.
[51] H. Ding, P. S. Kollipara, K. Yao, Y. Chang, D. J. Dickinson, Y. Zheng, *ACS Nano* **2023**, *17*, 9280.
[52] I. Hong, T. Anyika, C. Hong, S. Yang, J. C. Ndukaife, *ACS Photonics* **2023**, https://pubs.acs.org/doi/10.1021/acsphotonics.3c00983.
[53] P. Zhang, G. Song, L. Yu, *Photonics Res.* **2018**, *6*, 182.
[54] C. Hong, S. Yang, J. C. Ndukaife, *Nat. Nanotechnol.* **2020**, *15*, 908.
[55] S. Hu, Z.-W. Liao, L. Cai, X.-X. Jiang, *Phys. Status Solidi* **2020**, *217*, 1900604.
[56] J. Zhou, X. Dai, Y. Peng, Y. Zhong, H.-P. Ho, Y. Shao, B. Z. Gao, J. Qu, J. Chen, *Nano Res.* **2023**, *16*, 7710.
[57] A. P. Bregulla, A. Würger, K. Günther, M. Mertig, F. Cichos, *Phys. Rev. Lett.* **2016**, *116*, 188303.
[58] M. Zhang, X. H. Li, Y. D. Gong, N. M. Zhao, X. F. Zhang, *Biomaterials* **2002**, *23*, 2641.
[59] N. A. Alcantar, E. S. Aydil, J. N. Israelachvili, *J. Biomed. Mater. Res.* **2000**, *51*, 343.
[60] A. A. D'souza, R. Shegokar, *Expert Opin. Drug Delivery* **2016**, *13*, 1257.
[61] D. Niether, S. Wiegand, *J. Phys.: Condens. Matter* **2019**, *31*, 503003.
[62] M. Mohsen-Nia, H. Modarress, H. Rasa, *J. Chem. Eng. Data* **2005**, *50*, 1662.
[63] K. Devanand, J. C. Selser, *Macromolecules* **1991**, *24*, 5943.
[64] Y. T. Maeda, A. Buguin, A. Libchaber, *Phys. Rev. Lett.* **2011**, *107*, 038301.
[65] D. Vigolo, S. Buzzaccaro, R. Piazza, *Langmuir* **2010**, *26*, 7792.
[66] J. S. Donner, G. Baffou, D. Mccloskey, R. Quidant, *ACS Nano* **2011**, *5*, 5457.
[67] J. Zhou, X. Dai, B. Jia, J. Qu, H.-P. Ho, B. Z. Gao, Y. Shao, J. Chen, *Appl. Phys. Lett.* **2022**, *120*, 163701.
[68] M. Doi, S. F. Edwards, *The Theory of Polymer Dynamics*, Vol. *73*, Clarendon Press, Oxford **1988**.
[69] J. C. Giddings, P. M. Shinudu, S. N. Semenov, *J. Colloid Interface Sci.* **1995**, *176*, 454.

[70] P.-G. de Gennes, *Scaling Concepts in Polymer Physics*, Cornell University Press, Ithaca, NY **1979**.
[71] P. M. Bendix, S. N. S. Reihani, L. B. Oddershede, *ACS Nano* **2010**, *4*, 2256.
[72] L. Jauffred, A. Samadi, H. Klingberg, P. M. Bendix, L. B. Oddershede, *Chem. Rev.* **2019**, *119*, 8087.
[73] A. Qu, M. Sun, J.-Y. Kim, L. Xu, C. Hao, W. Ma, X. Wu, X. Liu, H. Kuang, N. A. Kotov, C. Xu, *Nat. Biomed. Eng.* **2021**, *5*, 103.
[74] I. Zare, M. T. Yaraki, G. Speranza, A. H. Najafabadi, A. Shourangiz-Haghighi, A. B. Nik, B. B. Manshian, C. Saraiva, S. J. Soenen, M. J. Kogan, J. W. Lee, N. V. Apollo, L. Bernardino, E. Araya, D. Mayer, G. Mao, M. R. Hamblin, *Chem. Soc. Rev.* **2022**, *51*, 2601.
[75] F. Li, J. Lu, X. Kong, T. Hyeon, D. Ling, *Adv. Mater.* **2017**, *29*, 1605897.
[76] D. Lu, G. Zhu, X. Li, J. Xiong, D. Wang, Y. Shi, T. Pan, B. Li, L. P. Lee, H. Xin, *Nat. Photonics* **2023**, *17*, 904.
[77] A. S. Urban, S. Carretero-Palacios, A. A. Lutich, T. Lohmüller, J. Feldmann, F. Jäckel, *Nanoscale* **2014**, *6*, 4458.
[78] H. Kuwata, H. Tamaru, K. Esumi, K. Miyano, *Appl. Phys. Lett.* **2003**, *83*, 4625.
[79] Y. Shi, D. Wang, Y. Xiao, T. Pan, D. Lu, G. Zhu, J. Xiong, B. Li, H. Xin, *Laser Photonics Rev.* **2022**, *16*, 2270062.
[80] J. W. Kang, P. T. C. So, R. R. Dasari, D.-K. Lim, *Nano Lett.* **2015**, *15*, 1766.
[81] Q. Zhan, *Opt. Express* **2004**, *12*, 3377.
[82] A. Lehmuskero, P. Johansson, H. Rubinsztein-Dunlop, L. Tong, M. Käll, *ACS Nano* **2015**, *9*, 3453.
[83] K. Svoboda, S. M. Block, *Opt. Lett.* **1994**, *19*, 930.
[84] D. M. Tscherne, C. T. Jones, M. J. Evans, B. D. Lindenbach, J. A. Mckeating, C. M. Rice, *J. Virol.* **2006**, *80*, 1734.
[85] Y. Yu, W. S. Zhang, Y. Guo, H. Peng, M. Zhu, D. Miao, G. Su, *Biosens. Bioelectron.* **2020**, *167*, 112482.
[86] B. Rudolph, K. M. Gebendorfer, J. Buchner, J. Winter, *J. Biol. Chem.* **2010**, *285*, 19029.
[87] J. Chen, Z. Kang, G. Wang, J. F. C. Loo, S. K. Kong, H.-P. Ho, *Lab Chip* **2015**, *15*, 2504.
[88] X. Chen, J. Chen, J. Zhou, X. Dai, Y. Peng, Y. Zhong, H.-P. Ho, B. Z. Gao, H. Zhang, J. Qu, Y. Shao, *Energy Rev.* **2023**, *2*, 100018.
[89] W. P. Wong, K. Halvorsen, *Opt. Express* **2006**, *14*, 12517.
[90] J.-H. Baek, S.-U. Hwang, Y.-G. Lee, *Mirror* **2007**, *685*, 61.